http://journals.aps.org/prl/abstract/10.1103/PhysRevLett.110.213001

Mapping (“seeing”) the Hydrogen atom wave function

PRL 110, 213001 (2013) PHYSICAL REVIEW LETTERS week ending 24 MAY 2013

Hydrogen Atoms under Magnification: Direct Observation of the Nodal Structure of Stark States

A. S. Stodolna,[1,*] A. Rouzée,[1,2] F. Lépine,[3] S. Cohen,[4] F. Robicheaux,[5]
A. Gijsbertsen,[1] J. H. Jungmann,[1] C. Bordas,[3] and M. J. J. Vrakking[1,2,*]

From Townsend, example of 2nd order, perturbation theory

$$\hat{H}_1 = e|\mathbf{E}|\hat{z}$$

z-hat is operator for z

$$\left[\hat{H}, \hat{L}_z\right] = 0$$

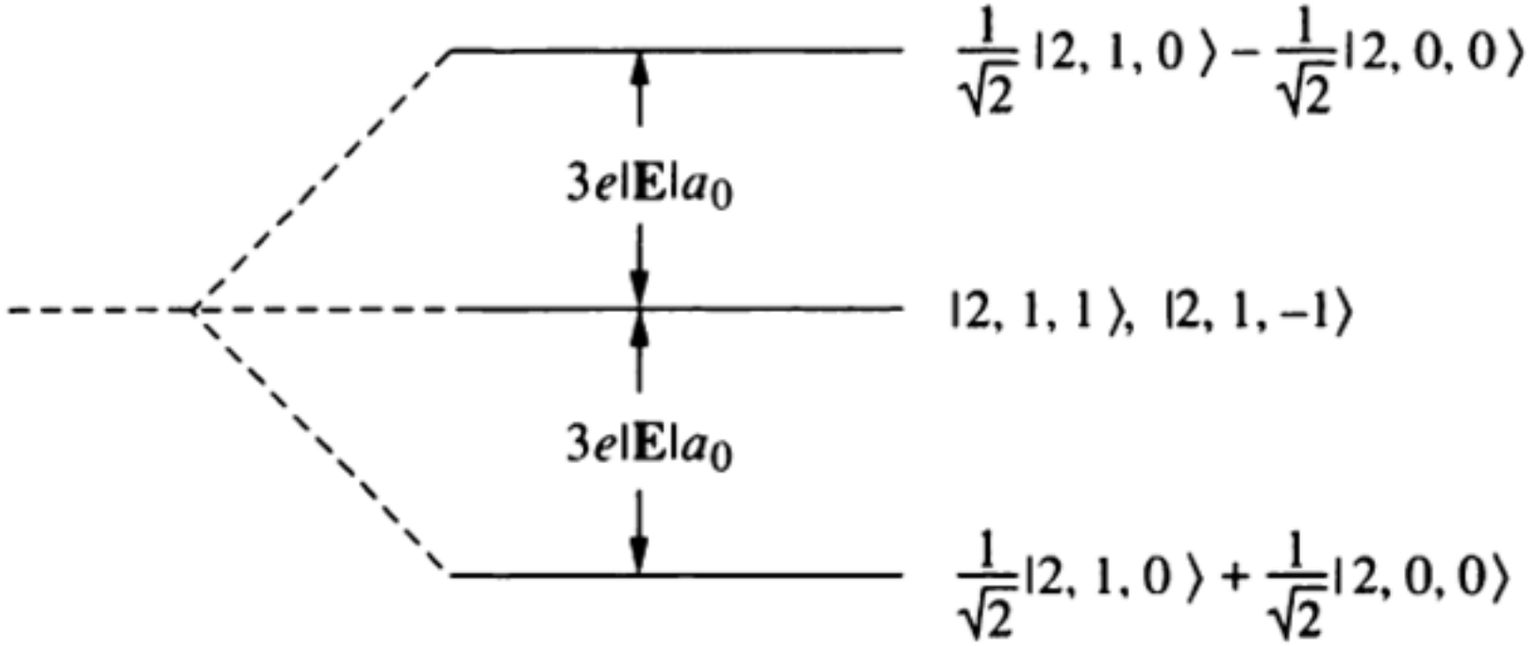

FIGURE 11.5
The first-order shifts in the energy levels of the $n = 2$ states of hydrogen in an external electric field.

Exactly solved in parabolic coordinates

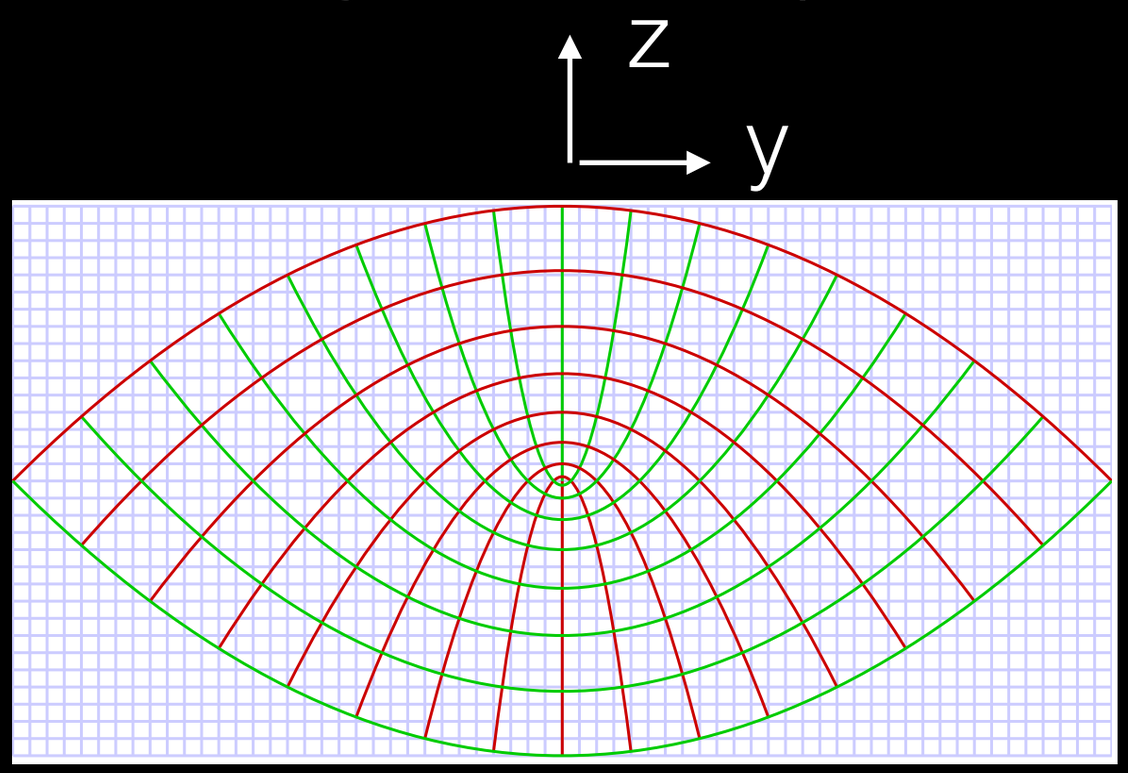

$$\xi = r - z = r(1 - \cos\theta)$$
$$\eta = r + z = r(1 + \cos\theta)$$
$$\phi = \phi$$

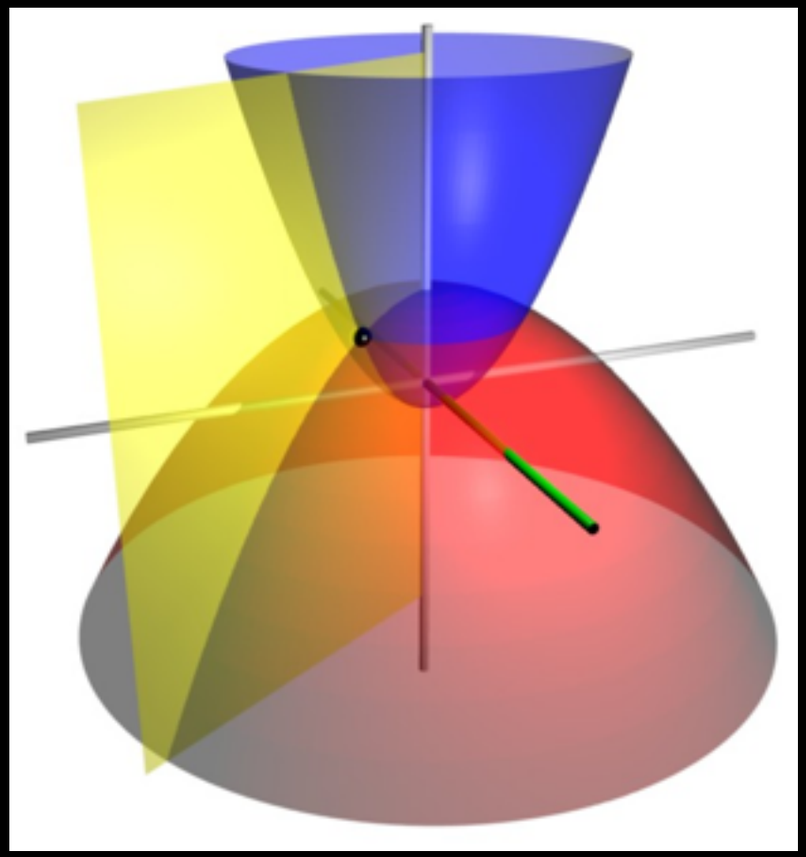

Friday Feature™, M. Gold

physics 492, Spring 2017

from Schiff, Quantum Mechanics

WAVE FUNCTIONS

It is clear from the foregoing discussion that the unnormalized hydrogen-atom wave functions in parabolic coordinates are

$$u_{n_1 n_2 m}(\xi,\eta,\phi) = e^{-\frac{1}{2}\alpha(\xi+\eta)}(\xi\eta)^{\frac{1}{2}|m|}L^{|m|}_{n_1+|m|}(\alpha\xi)L^{|m|}_{n_2+|m|}(\alpha\eta)e^{im\phi}$$

$$\alpha = \frac{\mu Z e^2}{\hbar^2(n_1 + n_2 + |m| + 1)}$$

For a particular energy level E_n and magnetic quantum number m ($n > |m|$), the parabolic quantum numbers n_1 and n_2 can be chosen such that $n_1 + n_2 = n - |m| - 1$, that is, in $n - |m|$ different ways. Similarly, for given n and m, the azimuthal quantum number l in the spherical solution can be chosen such that $|m| \leq l \leq n - 1$, and so also in $n - |m|$ different ways. Thus the $n - |m|$ products of the ξ and η functions are linear combinations of the $n - |m|$ products of the r and θ functions.

L are associated Laguerre polynomials, just as for solution in spherical coordinates

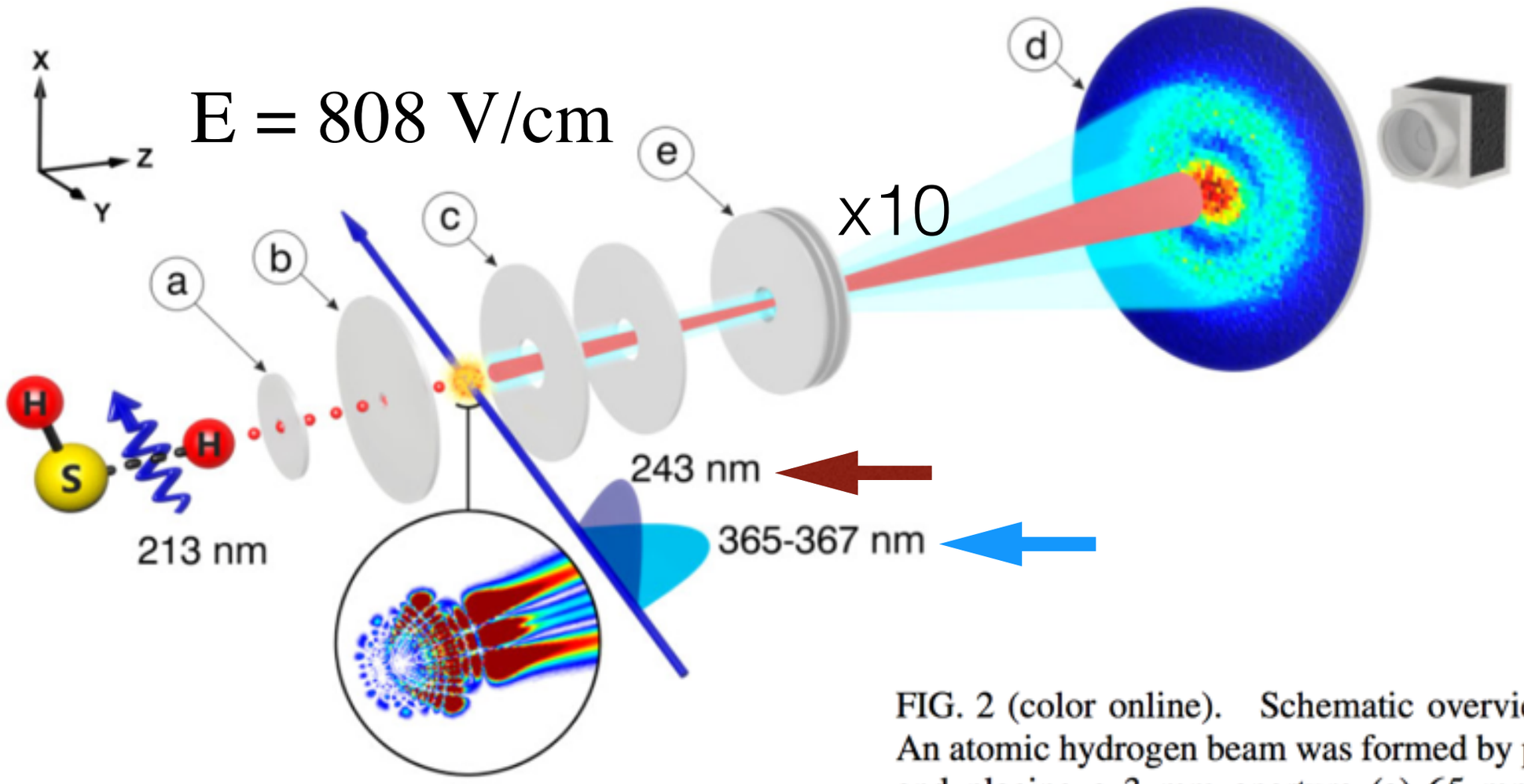

FIG. 2 (color online). Schematic overview of the experiment. An atomic hydrogen beam was formed by photodissociating H_2S and placing a 3 mm aperture (a) 65 mm downstream. In the active region of a velocity map imaging (VMI) spectrometer, the ground state hydrogen atoms were first excited to a mixture of $n = 2$ s and p states by a two-photon transition using a pulsed 243 nm laser. Next, they were ionized by a Fourier-limited, tunable (365–367 nm), UV laser. By applying a voltage difference across the repeller (b) and extractor (c) electrodes, the photoelectrons were accelerated towards a two-dimensional detector (d), consisting of a set of microchannel plates (MCPs), a phosphor screen and a CCD camera. En route to the MCP detector, the photoelectrons passed through a three-element Einzel lens (e), allowing an increase of the diameter of the recorded image by about one order of magnitude.

Friday Feature™, M. Gold

http://physics.aps.org/articles/v6/58

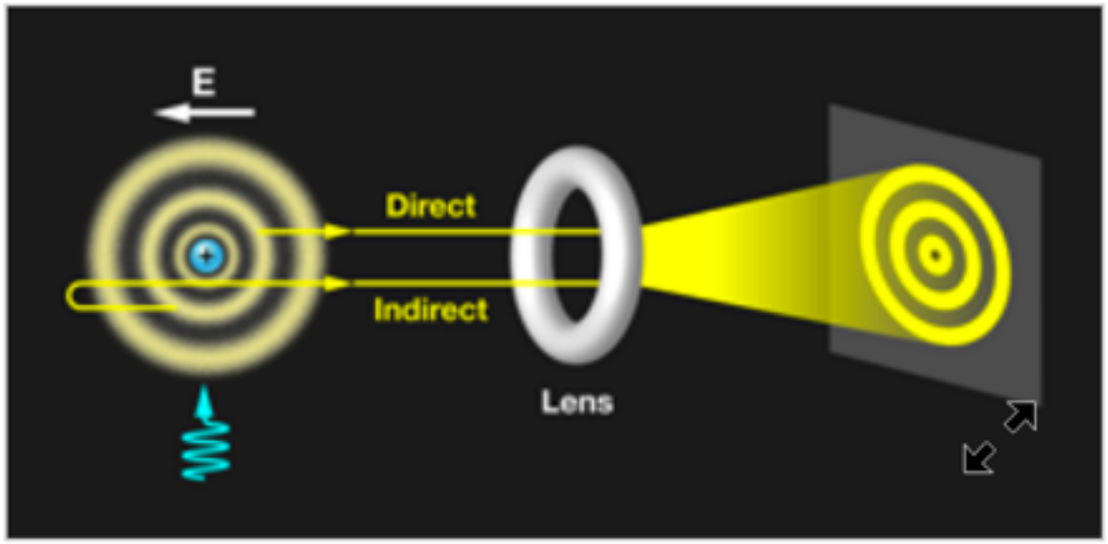

APS/Alan Stonebraker

Figure 1: A photoionization microscope provides direct observation of the electron orbital of a hydrogen atom. The atom is placed in an electric field E and excited by laser pulses (shown in blue). The ionized electron can escape from the atom along direct and indirect trajectories with respect to the detector (shown on the far right). The phase difference between these trajectories leads to an interference pattern, which is magnified by an electrostatic lens.

theory exp. comparison

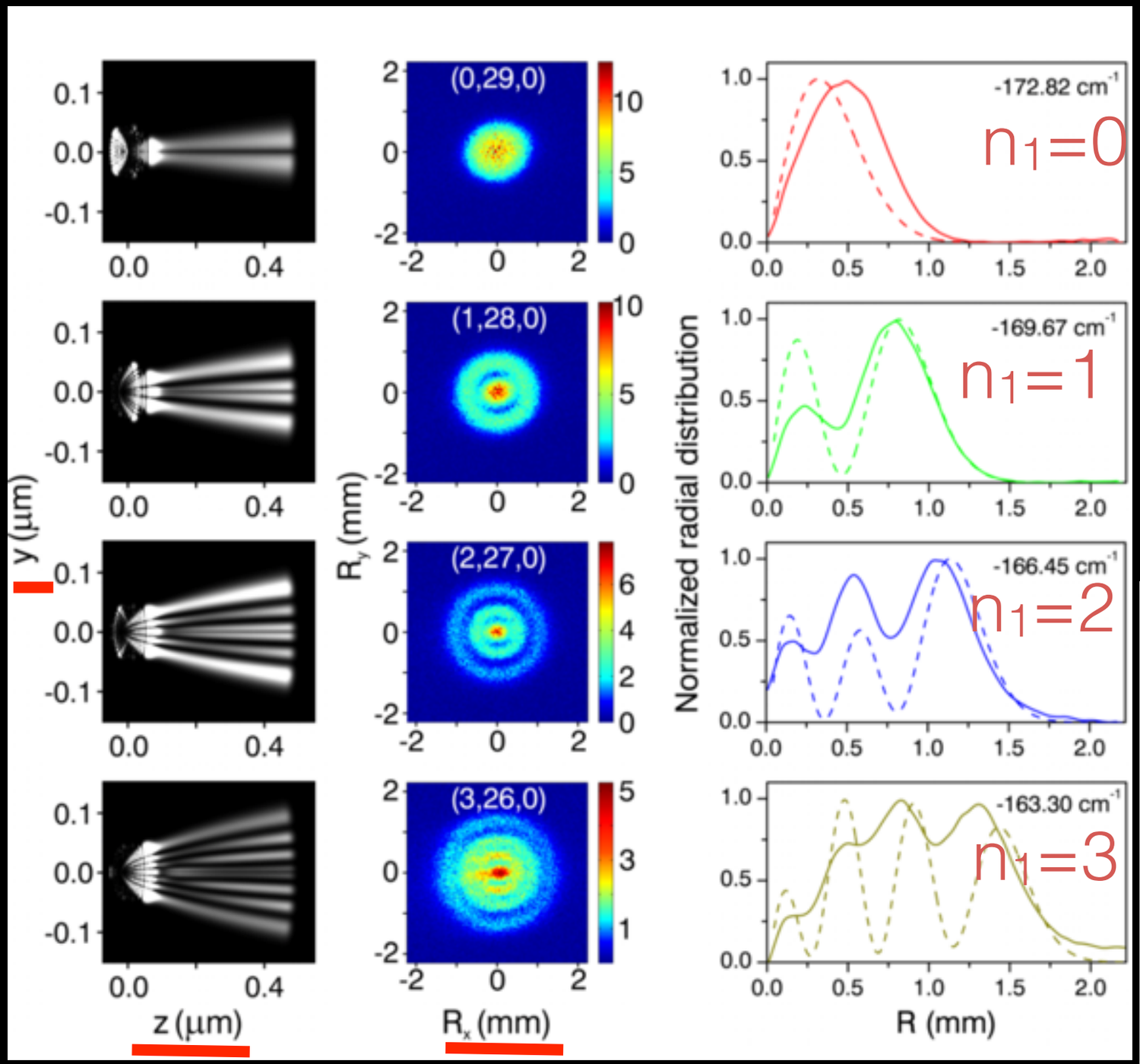

FIG. 3 (color online). Experimental observation of the transverse nodal structure of four atomic hydrogen Stark states. The images in the middle show experimental measurements for $(n_1, n_2, m) = (0, 29, 0)$, $(1, 28, 0)$, $(2, 27, 0)$, and $(3, 26, 0)$. Interference patterns are clearly observed where the number of nodes corresponds to the value of n_1. The results may be compared to TDSE calculations shown to the left (for details see text), revealing that the experimentally observed nodal structures originate from the transverse nodal structure of the initial state that is formed upon laser excitation. A comparison of the experimentally measured (solid lines) and calculated radial (dashed lines) probability distributions $P(R)$ is shown to the right of the experimental results. In order to make this comparison, the computational results were scaled to the macroscopic dimensions of the experiment. Please note that, since $P(R) = \int P(R, \alpha) R d\alpha$, the radial probability distributions $P(R)$ have a zero at $R = 0$, even if the two-dimensional images $P(R, \alpha)$ do not.

cross check: de-tune excitation laser,
Interference pattern disappears.

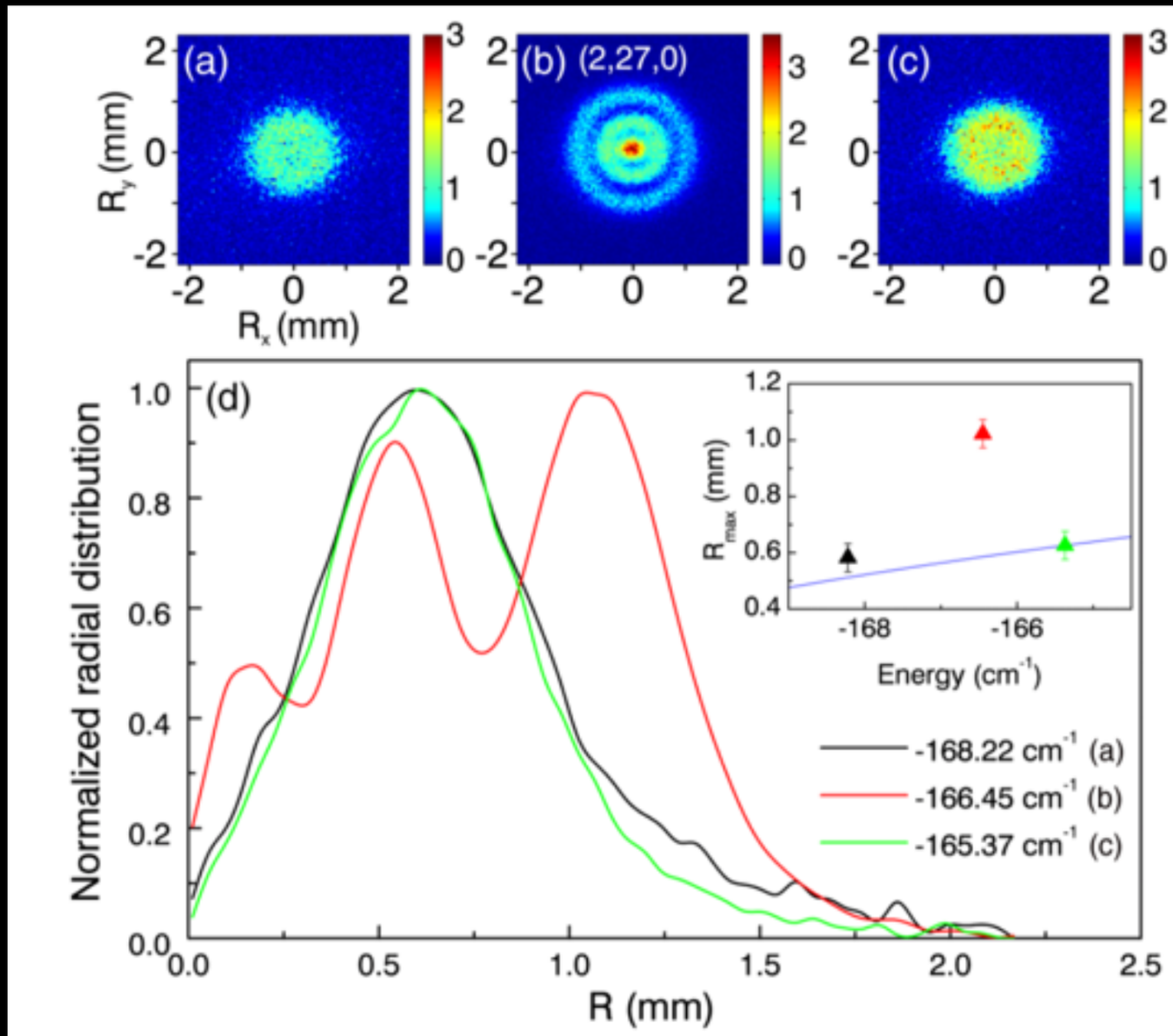

FIG. 4 (color online). Evidence for on-resonance ionization by tunneling through the Coulomb + static field potential. A comparison is shown between a measurement carried out for the $(n_1, n_2, m) = (2, 27, 0)$ resonance (b) and two non-resonant measurements performed 1.8 cm^{-1} below (a) and 1.1 cm^{-1} above (c) this resonance. The normalized radial distribution of the on- resonance measurement containing three maxima extends significantly further outward than the two off-resonance measurements which show only a single maximum (d). The inset in (d) shows a comparison of the radial extension of the experimental images, defined as the position of the outer maximum (color triangles) and the theoretical radial extension (blue, solid line) according to the classical formula (excluding tunneling contributions) $R_{\max} = [2L\frac{E-E_{sp}}{F}]^{1/2}$ [15], where L is the distance between the H atom and the detector ($L = 0.5$ m), and E_{sp} is the saddle point energy (-174.00 cm^{-1}). The experimental and theoretical radial extensions were matched for the measurement at $E = -165.37$ cm^{-1}.

http://journals.aps.org/prl/pdf/10.1103/PhysRevLett.110.183001

Lithium

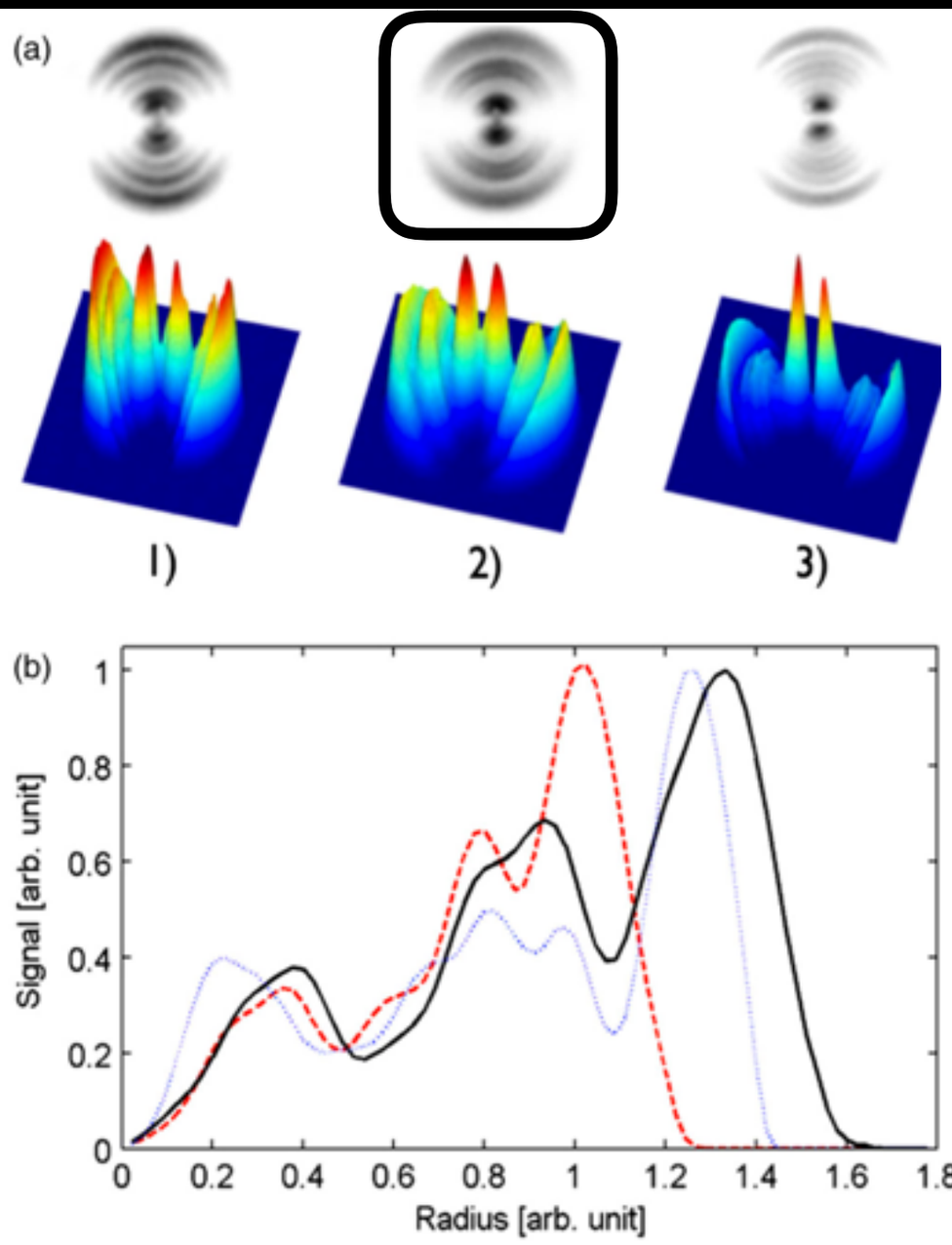

FIG. 3 (color online). (a) 2D and 3D representation of measured photoelectron images obtained in one-photon ionization of Li with $F = 1010$ V/cm, around the $(n_1^{\mathrm{res}} = 6,\ m = 1)$ resonance $(\varepsilon \equiv E/|E_{\mathrm{sp}}| = -0.789)$. (1) -19.78 meV ($\lambda = 230.800$ nm); (2) -19.07 meV ($\lambda = 230.769$ nm); and (3) -18.49 meV ($\lambda = 230.744$ nm). (b) Radial distribution of the images. The radius is scaled to the classical radius R_{max}^{cl} [12], whose size on the detector phosphor screen is ~6 mm. While in the non-resonant case, the radius of the image should smoothly increase with photon energy, we observe that the image is larger on-resonance (black continuous curve) and smaller at both lower (red-dashed line) and higher (blue-dotted line) photon energies. This is attributed to the tunneling ionization through the barrier.

backup

http://journals.aps.org/pra/pdf/10.1103/PhysRevA.94.013414

Lithium

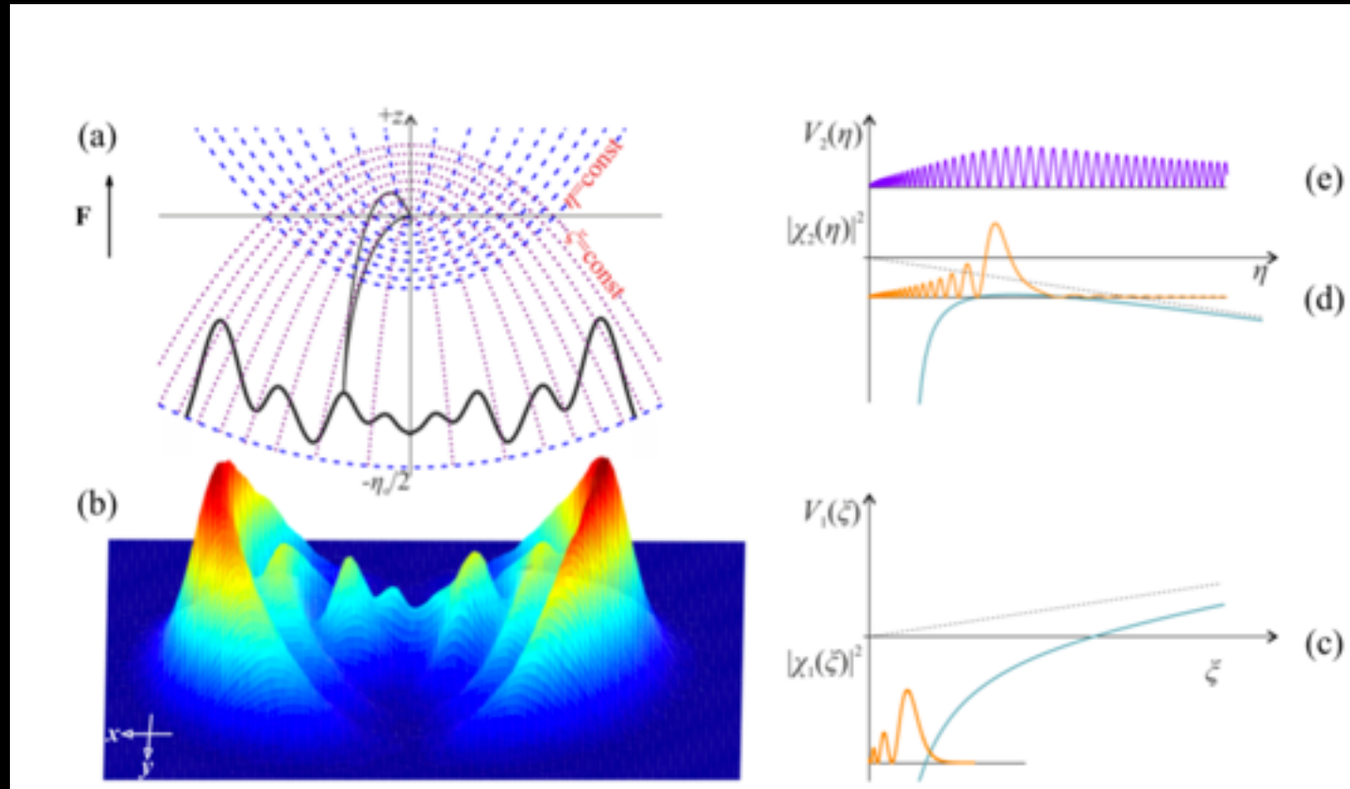

FIG. 1. Wave-function microscopy aims at observing the spatial structure of the electronic wave function. (a) The electron flux stemming from the photoionization of an atom in the presence of a static electric field is recorded perpendicularly to the field and at macroscopic distance, i.e., approximately along a given constant $\eta = \eta_o$ paraboloid. (b),(c) The image corresponds to the squared modulus of the wave function along the ξ coordinate where the electron motion is always bound. In (b) the nodes of the wave function are clearly observed in the example shown (with x and y denoting the detector plane), recorded with $F \approx 1\,\mathrm{kV/cm}$ and electron excitation energy exceeding E_{sp}^{cl} by 10 meV. Depending on the electron energy with respect to the maximum of the η potential, the classical electron motion may be either bound (d) or free (e). In the former case the electron can escape solely via tunneling and the image corresponds to a direct macroscopic projection of a quantum standing wave characterizing the quasibound electronic state (n_1^{res}, n_2^{res}, m) where the electron is initially localized within the inner η-potential well.

The presence of the dc field places the Rydberg electron above the classical ionization threshold but below the field-free ionization energy. The electron cannot exit against the dc field, but it is a free particle in many other directions. The outgoing electron wave accumulates a different phase, depending on the direction of its initial velocity. The portion of the electron wave initially directed toward the 2D detector (direct trajectories) interferes with the portion initially directed away from the detector (indirect trajectories). This produces an interference pattern on the detector. Stodolna *et al.* show convincing evidence that the number of nodes in the detected interference pattern exactly reproduces the nodal structure of the orbital populated by their excitation pulse. Thus the photoionization microscope provides the ability to directly visualize quantum orbital features using a macroscopic imaging device.

Potential energy

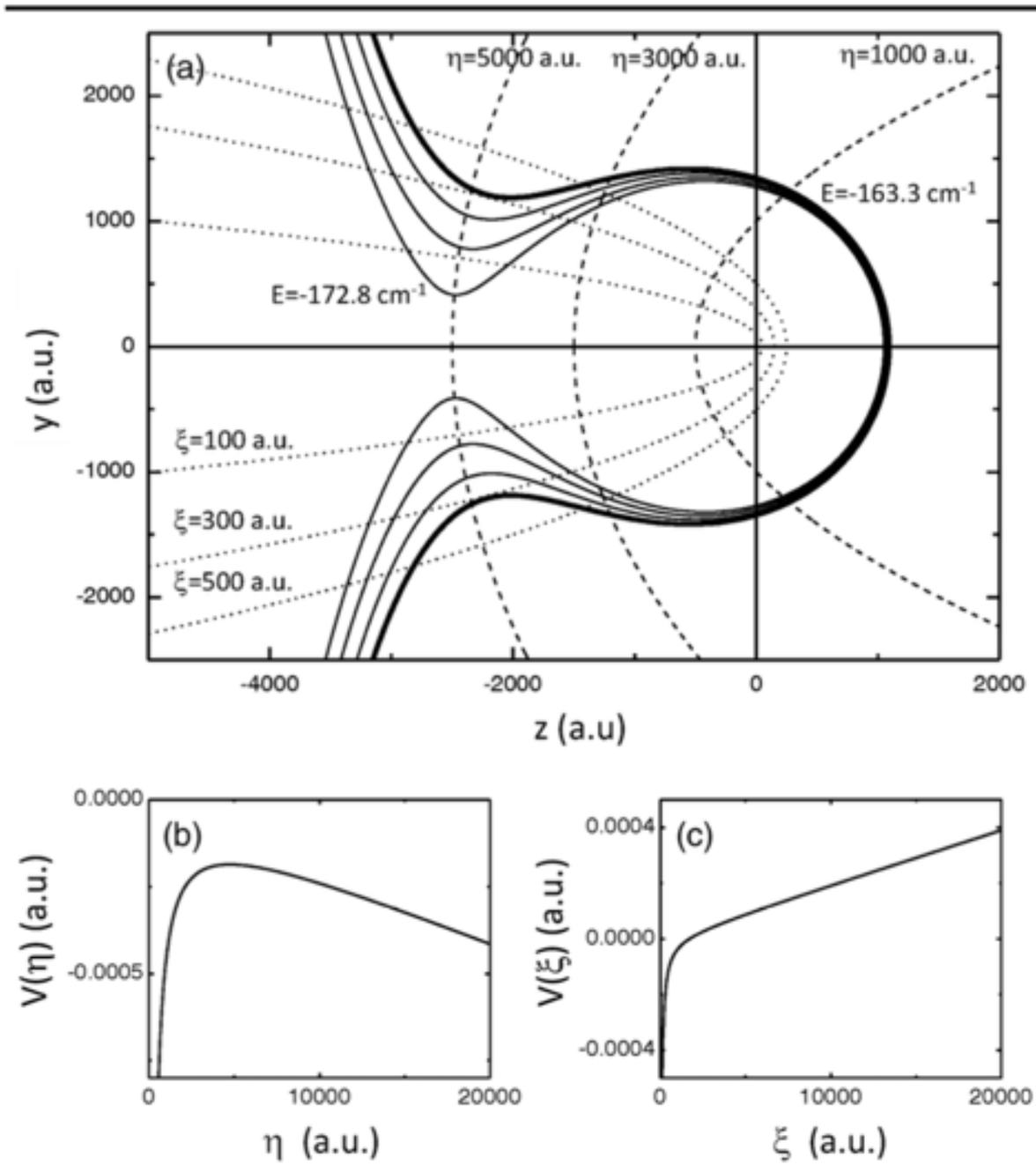

FIG. 1. (a) Potential energy landscape and relevant coordinate system for hydrogen atom photoionization microscopy in an 808 V/cm electric field (a.u. = atomic units). The hydrogen atom sits at the origin of the (z, y) coordinate system and the electric field is along the z axis. The boundary between the classically allowed and the classically forbidden region is plotted (solid lines) at the excitation energies of the four measurements that are shown in Fig. 3, i.e., ranging from $E = -172.8$ cm^{-1} to $E = -163.3$ cm^{-1} (thick outer solid line). Close to the saddle point, the electron can only escape through a very narrow gap in the Coulomb + dc field potential. The parabolic coordinates $\eta = r - z$ and $\xi = r + z$ are illustrated by plotting a series of contours at constant η (dashed lines) and ξ (dotted lines). The electron motion is always bound in the ξ coordinate whereas the motion along the η coordinate depends on the energy available for the η motion; (b) and (c) Potential energy curves $V(\eta) = -\frac{Z_2}{2\eta} + \frac{m^2-1}{8\eta^2} - \frac{F\eta}{8}$ and $V(\xi) = -\frac{Z_1}{2\xi} + \frac{m^2-1}{8\xi^2} + \frac{F\xi}{8}$, describing the motion along the η and ξ coordinates [11], where $Z_1 = (n_1 + \frac{|m|+1}{2})/n$ and $Z_2 = (n_2 + \frac{|m|+1}{2})/n$. $V(\eta)$ and $V(\xi)$ are shown for the $(n_1, n_2, m) = (3, 26, 0)$ quasibound state at $E = -163.3$ cm^{-1}.